

ON PREDICTING THE POLARIZATION OF LOW FREQUENCY EMISSION BY DIFFUSE INTERSTELLAR DUST

P. G. Martin¹

Abstract. Several of the current and next-generation cosmic microwave background (CMB) experiments have polarimetric capability, promising to add to the finesse of precision cosmology. One of the contaminating Galactic foregrounds is thermal emission by dust. Since optical interstellar polarization is commonly seen, from differential extinction by aligned aspherical dust particles, it is expected that thermal emission from these grains will be polarized. Indeed, in the Galactic plane and in dark (molecular) clouds, dust emission in the infrared and sub-millimetre has been measured to be polarized. It seems likely that the faint diffuse cirrus emission, of more relevance to CMB experiments, will be polarized too. We discuss how well the amount of polarization of this component can be predicted, making use of what is known about optical (and infrared and ultraviolet) interstellar polarization and extinction. Some constraints on the alignment of the carrier of the dust-correlated anomalous microwave emission can be made as well.

1 Introduction: CMB Polarization and Cirrus Contamination

Several of the current and next-generation cosmic microwave background (CMB) experiments have the capability of measuring linear polarization, a complementary probe for precision cosmology (e.g., Laureijs 2006; Polenta *et al.* 2005; Benoît *et al.* 2004; Prunet 2006). Among these experiments are Archeops (Benoît *et al.* 2004), BOOMERanG (B2K in 2003; Polenta *et al.* 2005; Netterfield 2006), and the Planck Surveyor (Laureijs 2006; Prunet 2006; Lammare *et al.* 2003). All-sky surveys by IRAS from 12 to 100 μm revealed faint diffuse emission (“cirrus”) everywhere, even at high Galactic latitudes (Low *et al.* 1984). One of the diffuse foregrounds contaminating the CMB signal is thermal emission by this diffuse interstellar dust (e.g., de Oliveira-Costa *et al.* 2004; Tucci *et al.* 2005), expected to correspond most closely spatially to the 100 μm emission (§ 2.1). This becomes

¹ Canadian Institute for Theoretical Astrophysics, University of Toronto;
e-mail: pgmartin@cita.utoronto.ca

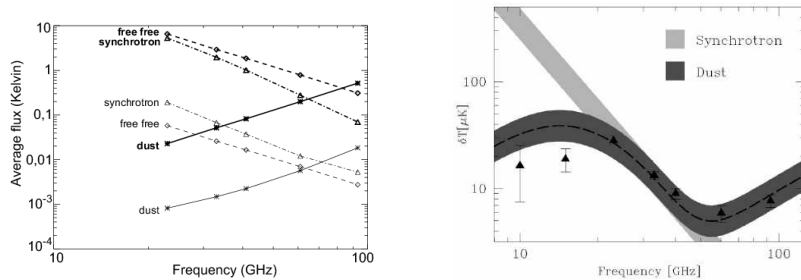


Fig. 1. Left: Foreground components contaminating the CMB at two representative latitudes. From www.planck.fr/heading136.html Giard & Lagache. Right: Alternative presentation from de Oliveira-Costa *et al.* (2004) showing the anomalous emission as well.

the dominant foreground above about 100 GHz ($\lambda < 3 \text{ mm} = 3000 \mu\text{m}$), and as the CMB fades toward higher frequencies, the rising dust spectrum becomes the dominant signal (Fig. 1). Where polarization is concerned, some further caution is needed in defining where the dust dominates. The frequency above which the polarized dust intensity exceeds the polarized synchrotron background is probably somewhat higher because the synchrotron component is likely to have a higher degree of polarization. Of course, it is the spatial fluctuations, which will vary from component to component, that are in the end important to CMB contamination. Multifrequency observations through the transitional range are therefore a prerequisite for separating these signals (component separation, not a specific topic of this paper; see e.g., Jaffe *et al.* 2004).

Some CMB experiments like B2K minimize cirrus contamination by concentrating measurements in regions of low foreground column density (Netterfield 2006). One strategy for cirrus mitigation could therefore be to mask out regions of bright cirrus. But only 20% of the sky has an HI column density below 10^{20} cm^{-2} (Miville-Deschênes, private communication) and even that produces a non-negligible foreground ($\sim 1 \text{ MJy sr}^{-1}$ at $100 \mu\text{m}$). The precision sought by instruments like the Planck Surveyor depends on broad sky coverage (Prunet 2006), and of course Planck will in any case produce data for the entire sky. Thus, as an alternative strategy, one needs to measure the properties of cirrus at higher frequencies where the CMB is not important, and then extrapolate to lower frequencies where one does have to address component separation. To inform/confirm the extrapolation, the cirrus properties at the lower frequencies can be assessed empirically in regions of brighter cirrus. The spectral properties of cirrus are of course an important diagnostic of the interstellar dust.

Since optical polarization is commonly seen, from differential extinction by aligned aspherical dust particles, it is expected that thermal emission from these grains will be polarized (Stein 1967). Indeed, in the Galactic plane and in dark (molecular) clouds, dust emission in the infrared and submillimetre has been measured to be polarized (Vaillancourt 2006; Hildebrand *et al.* 2000; Vaillancourt *et al.*

2003). In these dense regions, the interpretation of the polarization is complicated by many issues: beam dilution, distortions in the magnetic field topology, changes in the degree of alignment within clouds, grain evolution, and a range of grain temperatures and optical depth which affect which grains dominate the emission and polarization in various parts of the infrared to submillimetre spectrum. These are not considered here.

It seems likely that the faint diffuse cirrus emission will be polarized too, and this will not be affected by the above-mentioned complications. Diffuse dust polarization is of more relevance to CMB experiments. Polarimetric observations in the transitional high frequency range (see Table 1) were made by Archeops at 353 GHz (Benoît *et al.* 2004) and B2K and MAXIPOL at lower frequencies (Polenta *et al.* 2005; Johnson *et al.* 2003), precursors to Planck HFI. Archeops has reported detecting the dust polarization (§ refsobs). From the point of view of best examining the dust polarization, Planck has no polarimetric capability at 545 and 857 GHz where the dust polarized intensity would be the strongest. However, balloon-borne experiments like PILOT (Bernard 2005) and BLAST-pol will map the diffuse polarization with great sensitivity at higher frequencies.

This paper attempts to quantify the degree to which the diffuse dust emission is polarized, a contribution toward both component separation and dust physics.

WMAP (Kogut *et al.* 2003) and Planck have polarimetric capability at lower frequencies, down to 23 GHz and 30 GHz respectively, which can be used to examine the polarization of two other CMB foregrounds, synchrotron emission and the dust-correlated anomalous microwave (hereafter simply “anomalous”) emission (Draine & Lazarian 1998; Finkbeiner *et al.* 1999; Lazarian & Finkbeiner 2003; Finkbeiner 2004; Finkbeiner *et al.* 2004; de Oliveira-Costa *et al.* 2004; Davies 2006; Davis 2006). Some constraints on the alignment of a dust carrier of the latter emission, which would be diagnostic of the emission mechanism, are made

Table 1. Angular Resolution¹ of High-Frequency CMB Polarization Experiments

ν (GHz)	100	143	150	217	240	345	353	545	1250
λ (μm)	3300	2100	2000	1380	1250	870	850	550	240
Archeops							13		
BOOMERanG 2K			10		7	7			
MAXIPOL		10			10				
PILOT								2.3	1
Planck HFI	9.2	7.1		5			5		

¹ FWHM in arc minutes

here as well (§ 5.5).

1.1 A Legacy from Optical Polarization

Both optical interstellar polarization and polarization of thermal emission depend on aspherical (flattened or elongated) grains that are aligned. The orientation of the electric vector of the emitted radiation is along the long axis of the mean grain profile projected on the plane of the sky, while that of the optical polarization, being of transmitted light suffering differential extinction, is orthogonal to this. Particular ingredients in alignment theories are that grains are rapidly spinning about their axis of largest moment of inertia and that this is on average aligned with the Galactic magnetic field, so that consistent with observations the electric vector of optical polarization is along the direction of the projected magnetic field, while it is perpendicular for emission (see Fig. 2). There are several potentially viable alignment mechanisms as discussed elsewhere (Lazarian & Finkbeiner 2003; Lazarian & Yan 2004; Roberge 2004; Vaillancourt 2006) and in the Appendix. Nevertheless, it is still difficult to predict the degree of alignment with certainty *ab initio*, or as will become clear, gauge other important factors, and so a focus of this paper is to assess how well the degree of polarization of the diffuse cirrus component can be predicted semi-empirically.

To predict the degree of polarization of the dust-related CMB foreground(s), we draw on what can be deduced about alignment from optical (and infrared and ultraviolet) interstellar polarization and extinction, concentrating on diffuse dust associated with atomic gas. Still, it should be cautioned that the optical measurements are by necessity largely for column densities with $E_{B-V} > 0.1$ and so $N_H > 6 \times 10^{20} \text{ cm}^{-2}$. This corresponds to lines of sight with 100- μm cirrus brightness $I_{100} > 6 \text{ MJy sr}^{-1}$. While there will be many such directions

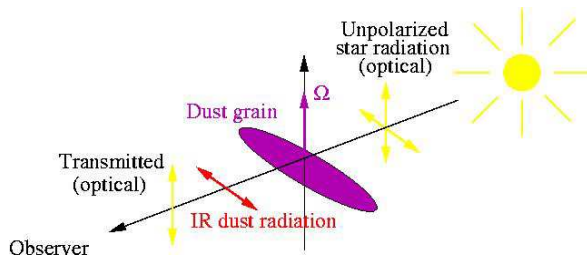


Fig. 2. The relationship of the polarization of emitted and transmitted radiation to the mean grain profile, aligned with respect to the Galactic magnetic field. In the far-infrared and submillimetre, there is more radiation emitted with polarization E-vector along the long axis. This is also the axis along which there is more extinction, and so the E-vector of the net transmitted radiation is orthogonal to this axis, and to the emitted polarization and the magnetic field. Graphic from Ponthieu & Lagache at www.planck.fr/article263.html.

in which to examine the polarization of the low-frequency foreground cirrus with forthcoming experiments, for CMB applications one needs to work at even lower column densities too. Another issue for any intercomparison of optical polarization and the polarization of low-frequency dust emission is that the Galaxy is optically thin for the latter. Therefore, we see the whole Galaxy, or right out of it, unlike probes with stars which rely on differential extinction along that path. But at high latitude, most relevant to the CMB, the effective paths might not be too dissimilar if the stars used were sufficiently distant.

A lot of attention goes into the degree of polarization $p = P/I$, the ratio of the polarized intensity P to the total emission I . Non-polarizing grains (or other emission components entirely) can contribute to I , potentially confusing the interpretation of any spectral dependence of p . We therefore also emphasize the importance of examining P and its spectral dependence directly, as a diagnostic of the aligned grains. P is of course what is relevant to the calculation of the power spectrum of the E and B modes of the polarized intensity. We do not attempt to predict these (Prunet *et al.* 1998; Tucci *et al.* 2005) since they depend in addition on the spatial variation of the degree and orientation of the alignment, whose statistical properties are not known (i.e., the statistics of P are different than the statistics of $p_{em}I$). However, the dust contribution to the power spectrum should scale with the same frequency dependence as P^2 (from dust), unless hoped-for “spatial – electromagnetic frequency decoupling” breaks down, i.e., there were different populations of grains with different alignment statistics whose relative contributions to P (and I) changed with frequency. A TE measurement of the dust emission at 353 GHz by Archeops (Ponthieu *et al.* 2005) provides a basis from which the potential contamination at lower frequencies can be estimated more directly.

2 Polarized Emission

The polarization of thermal emission by dust was first noted and estimated by Stein (1967). Hildebrand (1988) has since made more detailed calculations regarding infrared polarization and Hildebrand & Dragovan (1995) have analyzed far-infrared observations. We begin our estimate on the same basis, from electromagnetic scattering calculations of the cross-section for emission (equal to that for absorption), C_{em} , for single grains (for much of the rest of this section we suppress the subscript em). What is often computed for a single grain (e.g., Martin 1975) is an efficiency factor $Q = C/A$, where A is some measure of the area of the grain (whether projected or actual does not matter here). (Note that this is not Stokes Q .) But first we recall one of the challenges, that there are many different grain components potentially involved.

2.1 Grain Components: Lessons from IRAS and ISO

Interstellar extinction suggests a range of grain sizes and compositions (§ 3.1) and the infrared spectrum of cirrus in the range 3 to 1000 μm is interpreted as the sum

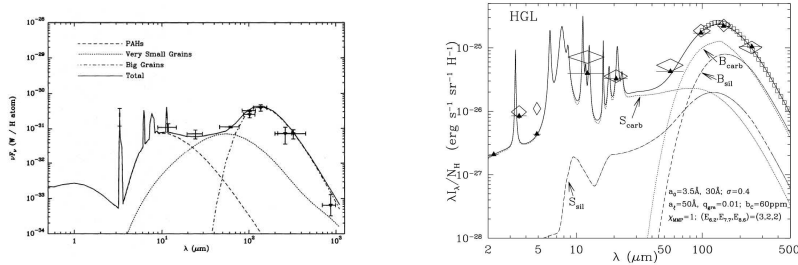


Fig. 3. Spectral components of high Galactic latitude cirrus in the infrared and implications for grain sizes. Left: Désert *et al.* (1990). Right: Li & Draine (2001). See text.

of several components too (Fig. 3).

Near 100 μm and longer, the range of interest here, the emission is thermal emission by “big” grains (size $\sim 0.1 \mu\text{m}$) in equilibrium with the local interstellar radiation field.

The mid-infrared emission at 60 and 25 μm is in excess of what can be attributed to the big grains, and is interpreted as non-equilibrium emission by grains that are very much smaller (VSGs: $0.007 \mu\text{m} = 70 \text{ \AA} = 7 \text{ nm}$), such that a single absorbed ultraviolet photon raises the temperature momentarily above the equilibrium value.

The 12 μm and shorter emission has many spectral features indicative of polycyclic aromatic hydrocarbons (PAHs). This can be thought of as either non-equilibrium emission by tiny grains/PAHs (1 nm) or the result of internal conversion in large molecules (see e.g., Draine & Li 2001).

All of these smaller grain components of course radiate at longer wavelengths too. But because the big grains contain most of the mass, it is they that dominate in the submillimetre.

Tiny grains (including PAHs) also spin rapidly and emit microwave radiation which could be another foreground contaminant of the polarized CMB, if aligned.

2.2 Submillimetre Spectrum: Total Intensity from an Ensemble of Grains

The emitted total intensity I summed over grain populations with column density N_g and temperature T_g , and acknowledging all “other” components (CMB, free-free, synchrotron, anomalous emission, point sources, etc.) is

$$I_\nu = \Sigma_g B_\nu(T) N A Q_\nu(T) = \Sigma_g B_\nu(T) N V \frac{C_\nu(T)}{V} + I_{\text{other}}. \quad (2.1)$$

Here C is the mean of the two effective cross sections for orientations of the electric vector parallel and perpendicular to the long axis of the projected mean profile of the aligned grains (“par” and “per” below in equation 2.2). Normally C depends on the grain size (characterized by some dimension a) but in the millimetre to

submillimetre range of interest, a is much smaller than the wavelength λ and the absorption cross sections per unit volume V , $C/V = Q/a$, is independent of a . The contributions to I (and P) are therefore weighted by the volume; in the diffuse interstellar medium, large grains carry most of the volume (or mass). It is often a good approximation in this limit that $C/V = Q/a = \alpha\nu^\beta$, where β is the spectral index of the emissivity (e.g., $\beta \sim 2$ for many materials) and α is the scaled opacity (with the basic frequency dependence removed), that varies from material to material. The thermal emission spectrum of each separate grain component is then a modified greybody emission, $\sim B_\nu(T)\nu^\beta$, with the appropriate T and β .

If there are multiple grain components with different properties (including alignment), then the contributions to I (and P) are weighted by the volume, α , and the Planck function at the appropriate temperatures, potentially making I deviate from a simple modified greybody with a frequency-independent β ; nor would β be necessarily representative (diagnostic) of any of the grain materials. Spectral changes would be most pronounced near the peak of any of the Planck functions, because of changing relative weights.

The wider the frequency range, the less likely it is that the opacity can be described by a single β . Changes in β with frequency over the range of interest are seen in laboratory experiments on amorphous silicates (Boudet *et al.* 2005). In fitting the spectrum, this provides an alternative to invoking an extra diffuse cold (< 10 K) dust component (Finkbeiner *et al.* 1999; Bourdin *et al.* 2002); although this provides a good fit and interpolation formula, one must be wary about taking the model literally, since dust that cold in the local diffuse ISM seems unphysical. Also there is the possibility, often ignored, that both α and β (thus the opacity) could be temperature dependent, again supported by the same laboratory measurements on amorphous materials, where the effects are attributed to intrinsic processes (two level systems, disordered charge distribution) in a single amorphous (silicate) material. This might also help explain why β appears to change with T (Boudet *et al.* 2005; Dupac *et al.* 2003), though here it can be noted that this is for T higher than in regions of relevance to diffuse CMB foregrounds. As discussed in § 5.4, an important implication might be that silicates provide a more dominant contribution to the emission at lower frequencies (§ 5.1), of relevance to polarized emission (and its detailed frequency dependence) since, among grain components, large silicates at least are aligned (§ 3.2).

2.3 Polarized Intensity

The emitted polarized intensity P (Stokes Q in the appropriately-rotated coordinate system) summed over all (aligned) grains, and including a shorter list of “other” polarized components, is similar:

$$P_{em} = -\sum_g B_\nu(T_g)N_g \frac{1}{2}(C_{par} - C_{per}) + P_{other}. \quad (2.2)$$

Since $C_{par} > C_{per}$, the emitted light is polarized with electric vector parallel to the long axis of the mean grain profile projected on the plane of the sky. The

minus sign invokes a convention, a reminder of the orthogonal orientation of the electric vector for emission relative to that of the transmitted light (see the sign convention in equation 3.1).

2.4 Emission Cross Sections for “Small” Particles

In the relevant limit in which a is much smaller than the wavelength λ simple analytical formulae can often be used. These are particularly straightforward to calculate for spheroids (or ellipsoids for that matter) that are homogeneous. In this limit there are only two principal cross sections to evaluate, corresponding to electric vector orientation parallel and perpendicular to the symmetry axis:

$$\frac{Q_{\parallel,\perp}}{a} = \frac{C_{\parallel,\perp}}{V} = -\frac{2\pi\nu}{c} \text{Im}\left(\frac{m^2 - 1}{L_{\parallel,\perp}(m^2 - 1) + 1}\right). \quad (2.3)$$

The principal cross sections are analytic functions of the complex refractive index m (hence dependent on grain material) and the “polarizability” factors L which depend on the shape and axial ratio (e.g., Martin 1975).

Interstellar grains are spinning and the largest amount of polarized emission P would arise for what we will call perfect spinning alignment (PSA), corresponding to rotation about the grain axis of largest moment of inertia, with all spin axes aligned along a common axis in space (the interstellar magnetic field) which in turn is in the plane of the sky.

For spheroids with perfect spinning alignment (PSA, as opposed to picket fence alignment, PF) we have $Q_{par,per} = Q_{\perp,\parallel}$ for oblate shapes and $Q_{par,per} = (Q_{\parallel,\perp} + Q_{\perp})/2$ for prolate shapes.

2.5 Degree of Polarization of Aligned Grains pa_{em}

For a single grain population (size, composition, and orientation, leading to the same temperature T_g), the dependences on $N_g V$ and $B_\nu(T_g)$ would cancel out in the ratio P/I and so

$$pa_{em} = -\frac{Q_{par} - Q_{per}}{Q_{par} + Q_{per}}. \quad (2.4)$$

In this simple situation, the degree of polarization is a property characteristic of the grains (composition, shape, alignment), but not their column density.

For m appropriate to “astronomical silicate” (Draine & Lee 1984; Rouleau & Martin 1991), Figure 4 illustrates pa_{em} calculated for several axial ratios. Also shown is one curve for an amorphous carbon material (AC1; Rouleau & Martin 1991).

There are several things to note. The degree of polarization is potentially very large, even from particles that are only mildly aspherical (axial ratio < 2). The value of pa_{em} depends on the shape, axial ratio, and degree of alignment, and so by itself is not diagnostic of the specific grain material. Even though Q/a has a strong spectral dependence as described above, this too cancels out in pa_{em} . There

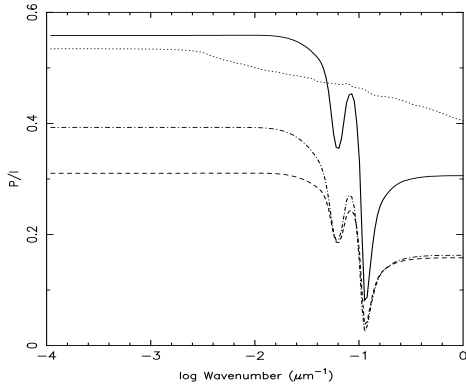


Fig. 4. pa_{em} for perfect spinning alignment, as a function of shape and composition. Silicate: oblate with axial ratio 1.4 (dash) and 2 (solid); prolate with axial ratio 2 (dash-dot). Amorphous carbon: oblate with axial ratio 2 (dots).

can be a slight frequency dependence of pa_{em} across the range of interest, due to changes in m .

In contrast, the spectral dependence of the observable P does retain the ν^β dependence. The wavelength dependence of optical polarization indicates that only large grains are preferentially aligned, which reinforces their dominance in the volume-weighted P and makes it more likely that the spectral dependence of P could be a useful diagnostic of the material of the aligned grains. For example, if over the range $\sim 100 - 1500$ GHz interstellar amorphous silicates had spectral index variations as measured by Boudet *et al.* (2005) or inferred by Li & Draine (2001) and these were the aligned grains (silicates certainly are aligned; see § 3.2), then this spectral behaviour would be imprinted directly on P with little effect on pa_{em} (see the illustration in § 5.4).

Non-aligned grains and I_{other} dilute the degree of polarization that would be produced by the aligned grains. The spectral dependence of P would not change, but the interpretation of p_{em} would become more difficult.

More generally still, spectral dependence in the net p_{em} can be introduced by frequency-dependent relative weighting in P and/or I , from different degrees of alignment, and/or temperatures T_g and opacities (many models implicitly imply these effects, e.g., Finkbeiner *et al.* 1999; Bourdin *et al.* 2002; Li & Draine 2001), and from the contributions P_{other} and I_{other} .

2.6 Challenges

As mentioned above, there is a wide range of grain sizes and compositions. In order to predict the polarized emission, we need to know which of these grains are aligned and how well. This is wrapped up with grain shape too: how flattened/elongated are the particles? In summary, p_{em} (and P) depends sensitively on axial ratio,

grain orientation, and composition, none of which are well known.

3 Optical (and Infrared and Ultraviolet) Interstellar Polarization

Fortunately, though the challenges can be met; the appropriate combinations of these unknowns can be constrained using interstellar polarization in the optical. First we reinforce one of the challenges, the multiple components suggested by interstellar extinction curve, $\tau_{ex}(\nu)$.

3.1 Grain Components: Lessons from the Extinction Curve

Interstellar extinction is caused by scattering plus absorption by grains comparable in size to the wavelength. The dependence of the cross sections C_{ex} on size and frequency cannot be obtained by the small particle approximation described above and require instead complex electromagnetic scattering calculations such as by Mie theory. The grain models are used to interpret observations of the interstellar extinction curve (Fig. 5, left).

One basic conclusion is that the continued rise in extinction into the ultraviolet requires smaller and smaller grains, a range already known prior to the interpretation of the infrared emission. There is a well-characterized "bump" at 2175 Å thought to arise in carbonaceous grains. This is another indication of separate grain components. In the infrared at 10 μm (Fig. 5, right), there is a prominent silicate absorption feature (Si-O stretch), the strength and shape of which requires that most of the available Si is depleted in amorphous silicate grains. The near-

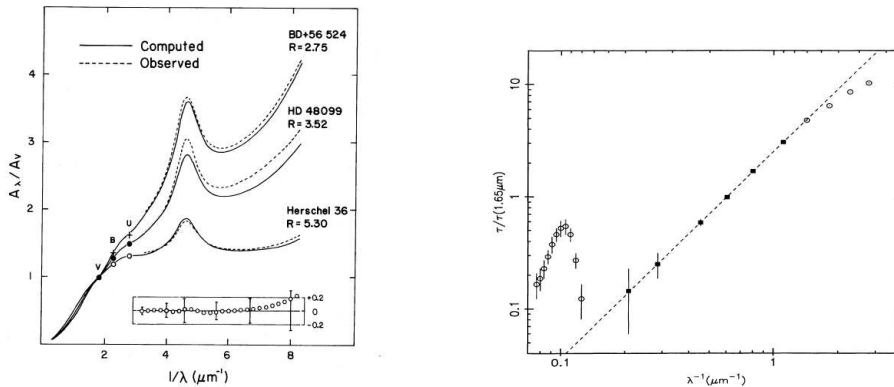


Fig. 5. Frequency dependence of interstellar extinction. Left: Extinction curves in the optical and ultraviolet showing a range of behaviour as a function of R_V (Cardelli *et al.* 1989); in the diffuse medium $R_V \sim 3.1$. The sole spectral feature is the prominent "bump" at 2175 Å. Right: In the infrared there is a power-law decrease, plus a distinctive 10- μm silicate feature (Martin & Whittet 1990).

infrared extinction follows a power law with index near 2 (Martin & Whittet 1990) which can be modeled as the scattering by large grains comparable in size to the wavelength.

In summary, grains come in many sizes (perhaps a function of composition). This raises many questions. Which grains produce the extinction in the optical and ultraviolet? Which grains produce the submillimetre emission? Which grains polarize in the optical and ultraviolet? Does this result in significant submillimetre polarization?

3.2 Lessons from the Polarization Curve

At least some of the grains are aspherical and aligned, so that in the plane of the sky the ensemble average grain profile is elongated, empirically with the long axis of this profile oriented perpendicular to the direction of the magnetic field B . Differential extinction, according to the orientation of the electric vector E with respect to the mean projected grain profile, produces a net polarization of transmitted light. Since there is greater extinction for E parallel to long axis, then E of the transmitted radiation is parallel to short axis, hence parallel to (Fig. 2).

Empirically, the “polarization curve”, the frequency dependent degree of polarization $p_{ex}(\nu)$, increases in the infrared to a peak in the optical and then declines into the ultraviolet (Fig. 6, left). Computations for single sizes indeed show a decline in polarization before the peak is reached in extinction (Roger & Martin 1979). But quantitatively this plus the continued rise of extinction into the ultraviolet, which implies smaller and smaller particles, plus the low ultraviolet

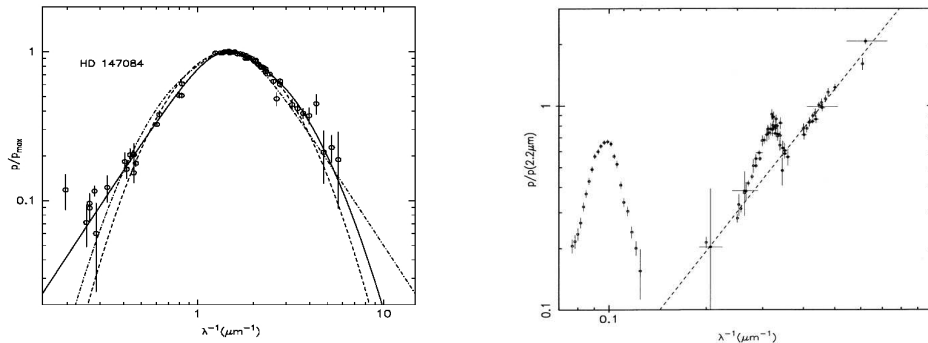


Fig. 6. Frequency dependence of interstellar polarization. Left: Polarization curve from the near-infrared to the ultraviolet, normalized to the maximum polarization in the visual (Martin *et al.* 1999). There is no strong ultraviolet polarization “bump” as in the extinction curve. Right: In the infrared there is a power-law decrease, plus a distinctive polarized 10- μm silicate feature (Martin & Whittet 1990). In lines of sight to an embedded source, such as this toward the Becklin-Neugebauer object in OMC 1, there is polarization at 3.1 μm ice band, interpreted as a thin frost on the aligned silicates.

polarization, leads to the important conclusion that only the larger grains are aspherical and aligned; the aligned grain mass distribution is very deficient in small particles (Kim & Martin 1995).

The strong 2175 Å bump does not have a correspondingly dramatic polarization feature at 2175 Å. A weak feature is seen only in two of the 28 lines of sight in the Galaxy observed by WUPPE and HST (FOS), despite having sufficient S/N (Martin *et al.* 1999). It is not a common phenomenon. The polarization feature is at the same position as the extinction bump, has a positive excursion, and shows no change in position angle. But it is at least two orders of magnitude smaller than the theoretical maximum for perfectly aligned graphite carriers (Martin *et al.* 1995). Thus, either the alignment is quite incomplete or only a small fraction of the grains is aligned. The result that the (presumed small) particles giving rise to the 2175 Å extinction bump are very poorly aligned is consistent with the poor alignment of the (other) small particles which give rise to the continuum ultraviolet extinction. A small residual alignment might be arise from the Davis-Greenstein process (Wolff *et al.* 1997).

Significantly, the feature at 10 μm is polarized (Fig. 6, right), indicating that at least the silicate grains are aspherical and aligned. Details of the relative changes of p_{ex} and τ_{ex} across the feature constrain the band strength and the shape and axial ratio; Hildebrand & Dragovan (1995) conclude that the silicate particles are oblate with axial ratio ~ 1.5 . It might be relevant that this is not unlike the individual sub-grains found in fluffy silicate agglomerate interplanetary dust particles, and the further insight from cometary material collected by Stardust is eagerly anticipated.

For embedded sources in molecular clouds, the polarized ice feature at 3.1 μm can be interpreted as a thin coating on the aligned silicates (as predicted: Martin 1975). The rise in the infrared is a power law (Martin & Whittet 1990; Martin *et al.* 1992) not unlike that for extinction, which again can be modeled as the (differential) scattering by large grains comparable in size to the wavelength (Kim & Martin 1995).

In summary, only the larger grains are aspherical and aligned. The 10 μm polarization shows that the silicate component is aligned, and the (oblate) particles have an axial ratio which is modest (near 1.5). It seems at least consistent (certainly adequate) to model the polarization with silicates alone.

3.3 Modeling

The observable $p_{ex}(\nu)$ increases with the column density of aligned grains. It is thus useful to normalize this out by considering the ratio with respect to extinction $\tau_{ex,\nu}$ which also builds up with column density. Suppressing the frequency dependence of the cross sections,

$$\left(\frac{p}{\tau}\right)_{ex} = \frac{\Sigma_g N_g \frac{1}{2}(C_{par} - C_{per})_{ex}}{\Sigma_g N_g \frac{1}{2}(C_{par} + C_{per})_{ex}} \quad (3.1)$$

(see, e.g., Martin 1974). This has a form that is deceptively like that for p_{em} , apart

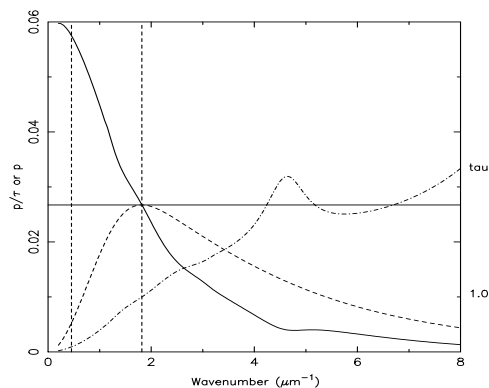


Fig. 7. Typical frequency dependence of $(p/\tau)_{ex}$ in the diffuse interstellar medium (solid curve). This is derived by dividing a typical polarization curve (dashed; Martin *et al.* 1999) by a typical extinction curve (dash-dot; Cardelli *et al.* 1989 for $R_V = 3.1$, normalized to $\tau_V = 1$, with scale on right). Both p_{ex} and $(p/\tau)_{ex}$ are normalized (scale on left) according to the maximum value observed at V (see Fig. 8). The ratio $(p/\tau)_{ex}$ at $2.2 \mu\text{m}$ (K band, left vertical dashed line) is significantly higher.

from the weighting of the latter with the Planck function (see equations 2.1 and 2.2, and 2.4). However, the further simplifications arising from the approximations for Q_{em} for small particles (e.g., simple volume weighting; size-independent behaviour) do not apply.

Figure 7 shows the very different frequency dependences of τ_{ex} (dash-dot) and p_{ex} (dash) derived from observations in the diffuse interstellar medium (??ccm, ??mar99). Both τ_{ex} and p_{ex} are sensitive to the actual size distributions, for all the grains and the subset that are aligned, respectively. Therefore, a self-consistent model to predict $(p/\tau)_{ex}$ and eventually p_{em} requires size distributions that reproduce the frequency dependence of both the polarization and extinction curves.

4 Constraining Alignment and Shape

Both the degree of alignment and shape influence the degree of polarization and so have to be constrained in order to predict p_{em} .

4.1 Imperfect Alignment

For the ensemble of grains, disalignment can be characterized by disorientation of the direction of the magnetic field along the line of sight, of the angular momentum vectors of the spinning grains with respect to the magnetic field, and of the spin axes (or body axes) with respect to the angular momentum vectors (e.g., Greenberg 1968; Purcell & Spitzer 1971; Martin 1975; Hildebrand 1988). These affect the

emission P and I , and p_{ex} and τ_{ex} , in subtly different ways.

For grains small compared to the wavelength, as appropriate for p_{em} , the cross sections for arbitrary orientations can be written as linear combinations of the principal cross sections, so that the average P and I over a distribution functions can be obtained more straightforwardly. For P the effects are actually separable, and not functions of shape, size, or composition, which can be useful; Greenberg (1968) gives a size-independent ‘‘Rayleigh reduction factor’’. Of course, in the general case, the appropriate sums in P over the grain components, which might have different alignment, still have to be performed. In the optical there are no such approximations, but there is some indication from representative calculations (e.g., τ_{green} , τ_{rogers}) that for the same disalignment the fractional reduction in p_{ex} is quite similar to that of P . Further calculations to quantify this would be of interest, but are beyond the scope of this paper.

There are related effects through the cross sections, which are not separable even for small particles, that tend to increase the emission I and τ_{ex} relative to perfectly aligned grains, further reducing p_{em} and $(p/\tau)_{ex}$, respectively. The effects are small for small axial ratios, but can be more substantial as grain flattening or elongation increases. As discussed below, in the interstellar medium even the maximum optical $(p/\tau)_{ex}$ corresponds to either axial ratios close to one, or close to random orientation for more elongated particles, with some independent evidence for the former. Thus for I and τ_{ex} calculations using spherical particles and/or random orientation might be close to appropriate. But without complete calculations for disaligned grains, this is one major source of systematic uncertainty in the applying ‘‘recipe’’ below (§ 4.3).

Relative to perfect spinning alignment (PSA), which for computational simplicity is often used, one can define a ‘‘reduction factor’’ R which quantifies how the polarization is reduced when the grains are less than perfectly aligned. From the discussion above, R_{ex} for $(p/\tau)_{ex}$ could be different than R_{em} for p_{em} and be frequency dependent. However, they are likely to be quite similar, and because little is actually known about the details of alignment, $R_{em} \simeq R_{ex}$ is a pragmatic approximation to adopt.

4.2 An Empirical Constraint

The observed amount of optical polarization per unit extinction provides an empirical measure of the asphericity and degree of alignment, whence R for a particular grain model with specified shapes and sizes.

Figure 7 shows $(p/\tau)_{ex}$ derived from the empirical curves for τ_{ex} and p_{ex} . There is a strong systematic spectral dependence. The normalization is for lines of sight in the interstellar medium for which the most optimal combination of shape and alignment is achieved (Fig. 8). This corresponds to a value $(p/\tau)_{ex} = 0.0267$ at the V passband or about 0.06 at K .

Hildebrand & Dragovan (1995) adopt a maximum, $p/\tau = 0.065$ at the K band. While this is from lines of sight with higher extinction, and perhaps higher density, observed by Jones *et al.* (1992), and so perhaps less appropriate to the cirrus

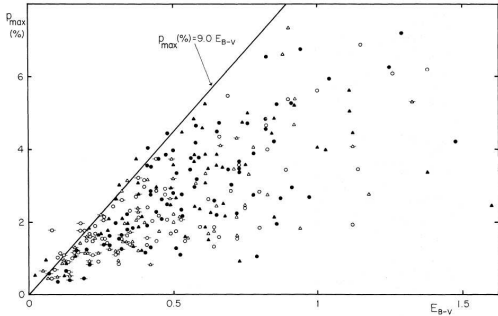


Fig. 8. Observed values of optical polarization near V plotted against colour excess E_{B-V} (Serkowski *et al.* 1975). For a typical ratio of total to selective extinction $R_V = 3.1$, the upper envelope corresponds to $(p/\tau)_{ex} = 0.0267$ at V or about 0.06 at the K band (Fig. 7). For directions in which the magnetic field is more along the line of sight, and/or for which there is a lower degree of alignment, $(p/\tau)_{ex}$ is lower, typically by a factor two, and p_{em} of the low frequency emission will be lower too.

application here, the value is nevertheless very similar.

4.3 A Bootstrapping Recipe

For their analysis of far-infrared polarization in more dense regions of the interstellar medium (clouds), complicated regions for which a maximum $p_{em} \sim 9\%$ is observed (Vaillancourt 2006; Hildebrand *et al.* 2000), Hildebrand & Dragovan (1995) gauge the effect of disalignment by first comparing p_{em} for their model at $2.2\ \mu\text{m}$ with $(p/\tau)_{ex}$ observed at $2.2\ \mu\text{m}$. In practice, there are two problems with their approach. First, they assumed that the formulae involving cross-sections for pure absorption would apply to both p_{em} in the far-infrared and $(p/\tau)_{ex}$ at K . However, the slope of the observed power-law dependence of extinction and polarization near K indicates that this involves grains of size comparable to the wavelength, where scattering is very important. The adopted formulae do not really apply at $2.2\ \mu\text{m}$. Second, even if this were the case, the evaluation of p_e near $2.2\ \mu\text{m}$ for silicates is very sensitive to how “dirty” they are, as quantified by the size of k , the imaginary part of the refractive index in the near-infrared and optical. This is poorly known. On the other hand, how “dirty” the silicates are is not relevant to the low frequency polarization. Therefore, for silicates, it is hard to bootstrap from the near-infrared to the far-infrared or submillimetre with confidence. Addressing the first problem with more realistic scattering models also eliminates the second.

To proceed, as stated in § 3.3 we must compute $(p/\tau)_{ex}$ according to equation 3.1 using realistic size distributions and an electromagnetic scattering theory (Mie-like) for particles comparable in size to the wavelength. This is not impossible, and so a practical bootstrapping recipe is (i) For a given axial ratio, and

perfect alignment, find the aligned grain size distribution by fitting the frequency dependence of interstellar polarization. Compare this to a consistent model of the frequency dependence of interstellar extinction, keeping track of the mass of all components (unaligned grains contribute to τ and not p , and so cause dilution). For this we use models by Kim & Martin (1995); only the silicates are aspherical and aligned, which is certainly adequate. (ii) Calculate $(p/\tau)_{ex}$ for this model (it can be evaluated for frequencies throughout the optical). We took the average of the two estimates in Table 1 of Kim & Martin (1995) and noted the implied substantial systematic error. (iii) Compare this to the observed maximum $(p/\tau)_{ex}$ (Fig. 7) to deduce a reduction factor $R_{ex} < 1$ reflecting the imperfect alignment. (iv) For the same model (shape, axial ratio, grain components), self-consistently calculate the polarization of the low-frequency thermal emission of the aligned grains, pa_{em} (e.g., Fig.4). (v) Assuming that $R_{em} = R_{ex}$, apply R from the interstellar polarization model for that axial ratio to find the expected maximum degree of polarization Rpa_{em} for the disaligned grains.

How robust this estimate is can be judged by repeating the recipe calculation for different shapes and axial ratios. (vi) There is a further complication, dilution of the polarization because of thermal radiation by non-aligned grains. This reduction factor $d < 1$ needs to be evaluated as self-consistently as possible (§ 5.1).

5 Results and Discussion

The results from the different steps of this recipe are collected in Table 2. There pa_{em} is evaluated at 350 GHz, but this choice is inconsequential (Fig. 4).

For perfectly aligned oblate silicate particles ($R \sim 1$ in this case), the axial ratio needs to be no higher than 1.4 to produce the maximum $(p/\tau)_{ex}$ observed. For

Table 2. Prediction of the Net Submillimetre Polarization

Axial ratio	Oblate			Prolate			
	$\sqrt{2}$	2	4	6	2^1	2^2	4^2
$(p/\tau)_{ex}$	0.04	0.08	0.12	0.12	0.05	0.09	0.14
R	0.67	0.36	0.23	0.23	0.53	0.30	0.19
pa_{em}^3	0.31	0.56	0.83	0.90	0.39	0.56	0.91
Rpa_{em}	0.21	0.20	0.19	0.21	0.21	0.17	0.17
$dRpa_{em}$ (%)	9.3	8.9	8.7	9.4	9.3	7.5	7.8

¹ perfect spinning alignment

² picket fence alignment

³ evaluated at 350 GHz

larger axial ratios, grains must be somewhat disaligned by a quantifiable amount ($R < 1$) to produce the same $(p/\tau)_{ex}$. The value of pa_{em} is large, and as expected higher for the more extreme axial ratios (Fig. 4). The application of the recipe to the models for axial ratios closer to unity is probably more reliable, and these ratios are possibly the most realistic as well. But it turns out that the product Rpa_{em} is fairly robust, depending little on the shape and axial ratio.

5.1 Dilution

Non-aligned grains contribute to the thermal emission and dilute the maximum polarization expected. The Kim & Martin models used involve silicates and (large) graphite particles (Kim *et al.* 1994), following Mathis *et al.* (1977) and Draine & Lee (1984). The relative contributions to the submillimetre emission can be judged from calculations by Draine & Anderson (1985), which do produce about the right amount of far-infrared emission per unit column density. This suggests quite a reduction, by $d \sim 1/3$. A more recent variant of this model, with slightly different size distributions and apportionment of material (Li and Draine 2001), gives $d \sim 0.58$ at 353 GHz (their Fig. 9). We adopt the mean, $d \sim 0.45$, and note another major contribution to the systematic uncertainty.

Note that the dilution of $(p/\tau)_{ex}$ in the optical by extinction by unaligned graphite (carbonaceous) particles has resulted in a larger R_{ex} , and so this low d can be considered as payback, compensating in the product dR . Likewise, if there were optical polarization by large carbonaceous particles, there would be an accompanying decrease in R but an increase in d , and so this change too would not produce a greatly different net p_{em} in the submillimetre.

5.2 Predicted Net Polarization p_{em}

This self-consistent model then predicts a maximum net polarization $dRpa_{em}$ as listed in Table 2 and summarized as the median $p_{em}(\%) = 8.9 \pm 0.7 \pm 3.5$. The result is not very dependent on the shape or axial ratio of the grains, as reflected in the modest rms 0.7% among the different models. The systematic uncertainty 3.5% is much more substantial, with the rough estimate based on actual application of the recipe to the models: calculating τ_{ex} appropriately (step (ii); § 4.1), the (frequency dependent) dilution d near 353 GHz (step (vi); § 5.1), and encompassing the assumption $R_{em} = R_{ex}$ (step (v); § 4.1).

Thus the maximum polarization to be expected is quite large, even without the possible boost accompanying spectral flattening of the amorphous silicate emissivity through 350 GHz.

But when averaged over large regions with (i) non-uniform alignment (beam dilution) or (ii) less than the optimal alignment, including the effects changes in the direction of the magnetic field, or unfavorable field orientation (something that changes systematically on a large scale in the Galaxy), or (iii) alignment which changes along the line of sight, then typically half of this might be expected,

judging from Fig. 8 which shows the depolarization from (ii) and (iii). This would still leave $p_{em} \sim 5\%$.

5.3 Observations

Benoît *et al.* (2004) present Archeops measurements of polarization in the Galactic plane at 353 GHz. They find $p_{em} \sim 4 - 5\%$ for the diffuse emission averaged over several square degrees and even higher values in some large clouds. The orientation of the E vector roughly perpendicular to the plane is reassuringly as expected. However, no clear correlation with optical interstellar polarization (for which the path lengths to the background stars would be shorter than for the emission) has been established and the data are not of high enough signal to noise to follow this at high resolution. Because of the long lines of sight and high column densities, the Galactic plane, even its diffuse emission, is probably not the best place to evaluate the polarization of the higher latitude cirrus foreground of the CMB. The amount of polarization observed is actually close to what is predicted by the analysis above. Although such estimates were actually made in 2003, before the Archeops results, this can hardly be taken as a triumph, given the large systematic uncertainties and the extra uncertainties of modeling the emission in the Galactic plane.

Nevertheless it does support the view that the polarization of the cirrus at higher latitude will be significant. Although the variations in alignment along and across the line of sight at high latitude are not known, it seems possible (because of the shorter paths and thus simpler geometry being integrated) that these variations will be less than in the Galactic plane, resulting in less depolarization.

5.4 Spectral Behaviour of p_{em} and P

As noted above, the spectral index of the amorphous silicate emissivity might be less steep than the $\beta \sim 2$ inherent in our calculations. A modest change was introduced by Li & Draine (2001, their eq. 1 and Fig. 9) to fit the frequency dependence of the diffuse emission. Boudet *et al.* (2005) suggest even stronger variations with frequency over the range 150 – 3000 GHz. In this case, the factor d would tend to increase with decreasing frequency as the relative importance of large silicates to the submillimetre emission rose. In models where it is the silicates that produce the polarization (subscribed to here), this frequency dependence of d would result in an increase in the net p_{em} at the lower frequencies and our estimate at 353 GHz could be low by a factor ~ 1.6 (not included in the systematic errors below). It will be interesting to learn the results from B2K (and Planck) which measure within this interesting range of frequencies.

Because of different weighting of different components, the spectral dependence of the polarized intensity P can be different than that of total emission, I (§ 2). Through dilution, non-aligned grains lower the net polarization. If the frequency dependence of emission for the diluting component is different, then this introduces a frequency dependence into $p_{em} = P/I$. We have just mentioned one example.

To characterize the intrinsic emission properties of the carriers of the polarization more directly, this confusion from dilution can be avoided in principle by examining P , which would isolate the spectral dependence of the polarizing emitters. For frequency ranges over which pa_{em} for this component could be assumed to be constant, this would directly give β , and its variations, for the spectral emissivity (I) of this aligned-grain component.

P is also the quantity on which to base statistical evaluation of the spatial variations.

A toy model for illustration is presented in Figure 9. Here it has been assumed that β for the aligned silicate component changes significantly with frequency, in the spirit of what has been inferred from astronomical observations and measurements in the laboratory (Boudet *et al.* 2005; J.-P. Bernard, private communication), although to be sure this is not (yet) well constrained. Specifically the model uses $\beta = 1.7$ for $\lambda < 1$ mm ($\nu > 300$ GHz), flattening (perhaps too abruptly in this illustrative model) to 0.5 through 2 mm (150 GHz), and then steepening to 1.5 (again for visual emphasis) beyond 5 mm ($\nu < 60$ GHz). For the silicate grains we take $T = 17$ K and $pa_{em} = 0.2$ (0.089/0.45 as in § 5.2). In a more realistic model there would be a slight increase in pa_{em} with decreasing frequency as a result of implied changes in the complex refractive index of the silicate. There is also an unpolarized graphite component with $T = 20.5$ K with relative emission such that $d = 0.45$ at 353 GHz (consistent with Table 2). For the graphite compo-

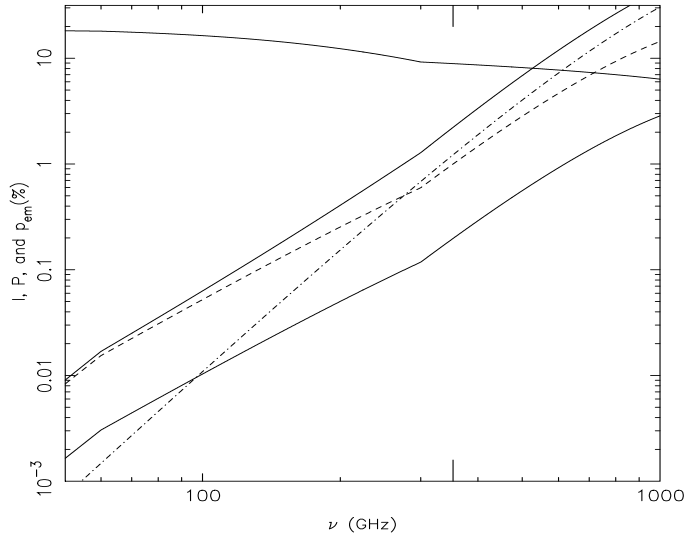


Fig. 9. Frequency dependence of observables p_{em} , I , and P (solid curves, from top) in an illustrative model in which the value of β for the amorphous silicate component varies with frequency (see text). The silicate and graphite contributions to I are shown by the dashed and dot-dash curves, respectively (for normalization, see text).

ment, $\beta = 2$. It should be kept in mind that the “graphite” might alternatively be amorphous carbon, in which some frequency dependent changes in β might also be expected.

The “observables”, I , P and p_{em} , are shown by the solid curves. in Figure 9. The model illustrates several important features. The spectral index measured from I is a function of frequency and would not be representative of either grain material. On the other hand, the spectral index measured from P would track that of the aligned amorphous silicates, even though this component is diluted in I . Toward lower frequencies silicates provide a more dominant contribution to the total emission (d is larger) and so even though pa_{em} does not rise significantly for this component, the net p_{em} does increase to lower frequencies.

It appears that the frequency dependence could be quite complicated, such that it would not be correct to extrapolate at constant β and/or p_{em} from measurements at a single high frequency toward the CMB frequencies. Rather, to disentangle this most convincingly, multi-frequency measurements of both p_{em} and P (and I) will need to be examined in regions of relatively bright foregrounds to produce a self-consistent model. Such an assessment of the dust polarization on the brighter cirrus, uncontaminated by the CMB at lower frequencies, would provide a basis for understanding the fainter cirrus contaminating the CMB. While this is not possible with Archeops, B2K and Planck have polarization capability at three frequencies and PILOT will extend this to higher frequencies (Table 1). It would be advantageous to make use of polarization measurements below 100 GHz too (e.g., WMAP and Planck), but at some point synchrotron emission, which probably has a higher intrinsic polarization, would no longer be negligible (Fig. 1), and there is the anomalous emission to consider too..

5.5 Alignment of Small Grains and Polarization of Anomalous Emission

As discussed in § 3.2, $(p/\tau)_{ex}$ is very low in the ultraviolet, where the extinction comes from small grains (VSGs, PAHs). What polarization there is (Fig. 7) is consistent with a fading contribution coming from big grains (Kim & Martin 1995). However, it is possible that there is a very low level of residual alignment of small grains, such as from the Davis-Greenstein process, could be present (Kim & Martin 1995; Wolff *et al.* 1997; Lazarian & Finkbeiner 2003).

Tiny grains, including if not exclusively PAHs, are the ones that could spin most rapidly to produce low frequency (~ 20 GHz) emission (Draine & Lazarian 1998), possibly accounting for the dust-correlated anomalous microwave emission (Finkbeiner 2004; Finkbeiner *et al.* 2004; de Oliveria-Costa *et al.* 2004; Davies 2006; Davis 2006). Since these small particles should not be well aligned, the degree of polarization of that component would not be high (tiny compared to the degree of polarization of the synchrotron component), a diagnostic feature that might be used to advantage by WMAP and Planck LFI. Still, the spectre of a few percent polarization for spinning dust could be a serious contamination for precise CMB polarization measurements (Lazarian & Draine 2000; Lazarian & Finkbeiner 2003).

We can be somewhat more quantitative in a semi-empirical if model-dependent way, starting from the Li & Draine (2001) model, in which PAHs are responsible for most if of the strong 2175 Å feature in the extinction curve (as reasonable and economical assumption). We then use the tight limits placed on the polarization of the 2175 Å feature (Martin *et al.* 1999; § 3.2). The relative change in polarization, compared to extinction, at the bump gives for this component $p/\tau_{ex} < 0.002$. The same quantity for perfectly aligned PAHs could be calculated using small-particle formulae as in equations 2.3 and 2.4 (the extinction is pure absorption), given a shape and refractive indices. However, there are no refractive indices since only absorptivity has been modeled (Li & Draine 2001), and for these large molecules it might not even be particularly appropriate. Nevertheless, since the PAHs are probably highly flattened, this quantity would be near unity, just as it is for tiny graphite spheroids of even modest asphericity (Martin *et al.* 1995; Wolff *et al.* 1997). Therefore, $R_{ex} < 0.002$. Similarly, for the rotational dipole emission of well aligned tiny grains, pa_{em} would also be unity. It would be reasonable to assume similar effects from disorientation: $R_{em} \sim R_{ex}$. Thus for the dust-related anomalous emission, we would predict a degree of polarization less than 0.2%, probably very much less given that polarization of the 2175 Å feature is unusual. This is more than an order of magnitude, probably nearer two, less than for the degree of polarization of the thermal dust emission, and also very much less than expected for synchrotron emission. The real situation is more subtle, however, because polarization of the rotational emission depends on the alignment of the angular momentum vector with respect to the magnetic field rather than the body axis with respect to the field, needed for the ultraviolet polarization (Lazarian & Draine 2000). If there is only partial alignment of the angular momentum vector and the body axis, then the low frequency polarization would be higher and with detection of polarization of the anomalous emission one might learn something more about the alignment.

To complicate things further, there is an alternative model for the anomalous microwave emission, magnetic-dipole emission from magnetic grains (Draine & Lazarian 1999; Lazarian & Finkbeiner 2003), which would have a very distinctive frequency-dependent polarization signature. Not enough is known about the properties of these grains or their alignment to make firm predictions of the degree of polarization. However, since magnetic inclusions might be a factor in grain alignment, this emission might be more closely related to “normal-sized” grains which are better aligned, and therefore might be more highly polarized than emission from spinning dust. Following similar bootstrapping arguments such as above, the order of magnitude might be like that given by Rpa_{em} in Table 2, thus $\sim 20\%$, reduced by other diluting contributions to the microwave emission. Again, synchrotron polarization would be a consideration.

This work was supported by the Natural Sciences and Engineering Research Council of Canada. I thank F. Boulanger, J.-L. Puget and colleagues for hospitality at IAS in 2003 where much of this work was done and F. Boulanger and M.-A. Miville-Deschênes for encouraging me to publish the results!

This volume is *Sky Polarisation at Far-infrared to Radio Wavelengths: The Galactic Screen before the Cosmic Microwave Background*, eds. M.-A. Miville-Deschênes and F. Boulanger. EAS Publications Series, Vol. –: Paris

References

- Benoît, A., et al. 2004, *A&A*, 424, 571
- Bernard, J.-P. 2005, *17th ESA Symposium on European Rocket and Balloon Programmes and Related Research*, ESA SP-590, 587. See also www.cesr.fr/~bernard/PILOT
- Boudet, N., Mutschke, H., Nayral, C., Jäger, C., Bernard, J.-P., Henning, T., & Meny, C. 2005, *ApJ*, 633, 272
- Bourdin, H., Boulanger, F., Bernard, J.-P., & Lagache, G. 2002, *ApSpS*, 281, 243
- de Oliveira-Costa, A., Tegmark, M., Davies, R. D., Gutiérrez, C. M., Lasenby, A. N., Rebolo, R., & Watson, R. A. 2004, *ApJ Letters*, 606, L89
- Dupac, X., et al. 2001, *ApJ*, 553, 604
- Dupac, X., et al. 2003, *A&A*, 404, L11
- Cardelli, J. A., Clayton, G. C., & Mathis, J. S. 1989, *ApJ*, 345, 245
- Davies, R. 2006, EDP (this volume)
- Davis, R. J. 2006, EDP (this volume)
- Désert, F.-X., Boulanger, F., & Puget, J. L. 1990, *A&A*, 237, 215
- Draine, B. T., & Anderson, N. 1985, *ApJ*, 292, 494
- Draine, B. T., & Lazarian, A. 1998, *ApJ*, 508, 157
- Draine, B. T., & Lazarian, A. 1999, *ApJ*, 512, 740
- Draine, B. T., & Lee, H. M. 1984, *ApJ*, 285, 89
- Draine, B. T., & Li, A. 2001, *ApJ*, 551, 807
- Finkbeiner, D. P., Davis, M., & Schlegel, D. J. 1999, *ApJ*, 524, 867
- Finkbeiner, D. P. 2004, *ApJ*, 614, 186
- Finkbeiner, D. P., Langston, G. I., & Minter, A. H. 2004, *ApJ*, 617, 350
- Greenberg, J. M. 1968, *Nebulae and Interstellar Matter*, eds., B. M. Middlehurst & L. M. Aller (Chicago: University of Chicago), 221
- Hildebrand, R. H. 1988, *QJRAS*, 29, 327
- Hildebrand, R. H., & Dragovan, M. 1995, *ApJ*, 450, 663
- Hildebrand, R. H., Davidson, J. A., Dotson, J. L., Dowell, C. D., Novak, G., & Vaillancourt, J. E. 2000, *PASP*, 112, 1215
- Jaffe, A. H., et al. 2004, *ApJ*, 615, 55
- Johnson, B. R., et al. 2003, *New Astronomy Review*, 47, 1067
- Jones, T. J. 1989, *ApJ*, 346, 728
- Jones, T. J., Klebe, D., & Dickey, J. M. 1992, *ApJ*, 389, 602
- Kim, S.-H., & Martin, P. G. 1994, *ApJ*, 431, 783
- Kim, S.-H., & Martin, P. G. 1995, *ApJ*, 442, 172
- Kim, S.-H., & Martin, P. G. 1995, *ApJ*, 444, 293
- Kim, S.-H., Martin, P. G., & Hendry, P. D. 1994, *ApJ*, 422, 164
- Kogut, A., et al. 2003, *ApJ Supp*, 148, 161
- Lamarre, J. M., et al. 2003, *New Astronomy Review*, 47, 1017

- Laureijs, R. 2006, EDP (this volume)
- Lazarian, A., & Draine, B. T. 2000, ApJ Letters, 536, L15
- Lazarian, A., & Finkbeiner, D. 2003, New Astronomy Review, 47, 1107
- Lazarian, A., & Yan, H. 2004, ASP Conf. Ser. 309: Astrophysics of Dust, 309, 479
- Li, A., & Draine, B. T. 2001, ApJ, 554, 778
- Low, F. J., et al. 1984, ApJ Letters, 278, L19
- Martin, P. G. 1974, ApJ, 187, 461
- Martin, P. G. 1975, ApJ, 202, 393
- Martin, P. G. *et al.* 1992, ApJ, 392, 691
- Martin, P. G. *et al.* 1995, *The Diffuse Interstellar Bands*, eds., A. G. G. M. Tielens & T. P. Snow (Dordrecht: Kluwer), 271
- Martin, P. G., Clayton, G. C., & Wolff, M. J. 1999, ApJ, 510, 905
- Martin, P. G., & Whittet, D. C. B. 1990, ApJ, 357, 113
- Mathis, J. S., Rumpl, W., & Nordsieck, K. H. 1977, ApJ, 217, 425
- Netterfield, C. B. 2006, EDP (this volume)
- Polenta, G., et al. 2005, Advances in Space Research, 36, 1064
- Ponthieu, N., et al. 2005, A&A, 444, 327
- Prunet, S., Sethi, S. K., Bouchet, F. R., & Miville-Deschênes, M.-A. 1998, *â*, 339, 187
- Prunet, S. 2006, EDP (this volume)
- Purcell, E. M. & Spitzer, L. Jr. 1971, ApJ, 167, 31
- Roberge, W. G. 2004, ASP Conf. Ser. 309: Astrophysics of Dust, 309, 467
- Rogers, C., & Martin, P. G. 1979, ApJ, 228, 450
- Rouleau, F., & Martin, P. G. 1991, *Extreme Ultraviolet Astronomy*, eds., R. F. Malina & S. Bowyer (Oxford: Pergamon), 341
- Rouleau, F., & Martin, P. G. 1991, ApJ, 377, 526
- Serkowski, K., Mathewson, D. L., & Ford, V. L. 1975, ApJ, 196, 261
- Stein, W. A. 1967, ApJ, 148, 295
- Tucci, M., Martínez-González, E., Vielva, P., & Delabrouille, J. 2005, MNRAS, 360, 935
- Vallée, J. P. 2003, New Astronomy Review, 47, 85
- Vaillancourt, J. E. 2006 EDP (this volume)
- Wolff, M. J., Clayton, G. C., Kim, S.-H., Martin, P. G., & Anderson, C. M. 1997, ApJ, 478, 395

Appendix: The Last Word – Grain Alignment Explained

I recommend looking at the above-mentioned Planck web pages, but one thing that cannot be found there is an explanation of why the grains are aligned. Recall that somehow the dust particles are supposed to be spinning preferentially around the magnetic field. At the conference I announced my forthcoming monograph “Alignment for Dummies” (coming soon to a discerning supermarket checkout counter near you) and to pique curiosity further (advanced sales benefit from feverish anticipation) I elaborated on the merits of one new theory of grain alignment. It turns out that the new theory is rather straightforward, so much so that I attempted to explain it *en français*, hoping to motivate, indeed enable, Lagache and colleagues to update their Planck web pages.

C'est facile, comme “un, deux, trois.”

Un! Voila, une grande poussière. Je pense que c'est organique, à la Greenberg.



Fig. 10. A moment of great anticipation in the demonstration of “Intelligent Alignment,” at the point of “contact” as the propeller motion is energized.

Deux! Voilà, le champs magnétique interstellaire – plus grand que les Champs-Élysée.

Mais, aucun alignement! Dommage!

Trois! Voilà, la main de Dieu!

Alors, attention! Un: une poussière. Deux: un champs magnétique. Trois: la main de Dieu. Alignement!

The live demonstration (Fig. 10) does benefit from a grocery bag containing appropriate ingredients! Any good theory needs a name and it is suggested that this theory might well merit the status of “Intelligent Alignment.”